International Journal of Fracture **125:** 307–333, 2004.

Failure criteria for brittle elastic materials

ZOHAR YOSIBASH, ARIE BUSSIBA and ILAN GILAD
Pearlstone Center for Aeronautical Engineering Studies, Department of Mechanical Engineering, Ben-Gurion University of the Negev, Beer-Sheva 84105, Israel. E-mail: zohary@bgumail.bgu.ac.il

Received 28 November 2002; accepted in revised form 8 December 2003

Abstract. The validity of several known failure initiation criteria at reentrant corners in brittle elastic materials is examined and a simple one is proposed. Their predictions, under mode I stress field, are compared to experimental observations carried out on PMMA (polymer) and Alumina-7%Zirconia (ceramic) V-notched specimens. Because all realistic V-notched reentrant corners are blunt, a detailed experimental procedure has been followed, focusing on specimens with different notch tip radii. It is demonstrated that by assuming a sharp V-notch, some failure criteria predict reasonably well the experimental findings, and that corrections are needed in order for these to take into consideration the realistic radius at the notch tip.

Key words: Failure initiation, generalized stress intensity factors, V-notch.

Abbreviations: SED – strain energy density; GSIF – Generalized stress intensity factor.

1. Introduction

The successful use of linear elastic fracture mechanics theory in predicting brittle fracture in isotropic cracked solids is attributed to the successful correlation of a single parameter, namely the stress intensity factor, with experimental findings. For cracks in two-dimensional domains made of isotropic materials, it is associated with the first coefficient in the expansion of the displacements field in the vicinity of a crack tip, given by the following expression (see Williams, 1952):

$$\mathbf{u} = \sum_{\ell=1}^{L} A_\ell \, r^{\alpha_\ell} \begin{Bmatrix} u_1^{(\ell)}(\theta) \\ u_2^{(\ell)}(\theta) \end{Bmatrix} + \mathbf{u}_{\text{reg}} = \sum_{\ell=1}^{L} A_\ell \, r^{\alpha_\ell} \mathbf{u}^{(\ell)}(\theta) + \mathbf{u}_{\text{reg}}, \tag{1}$$

where (r, θ) are cylindrical coordinates of a system located in the crack tip and it involves only integer and half-integer powers. The first two exponents α_1 and α_2 are equal to $1/2$, and the functions $u_1^{(\ell)}(\theta)$ and $u_2^{(\ell)}(\theta)$ are known explicitly. L may be taken as large as required, and the remainder $\mathbf{u}_{\text{reg}}$ is a vector of smooth functions. Usually 'mode I' stress intensity factor, $K_I = A_1 * \sqrt{2\pi}$ associated with the 'symmetric crack mode', determines the onset of failure: i.e. when it equals K_{Ic} (a material dependent parameter) fracture occurs. This onset of failure criteria has been first suggested by Irwin (1957). The feasibility of using the single parameter K_{Ic} (material dependent value) to determine the onset of failure is a result of the universal nature of the stress tensor in the vicinity of the crack tip. For crack tips, under mode I loading, a duality exists between the Irwin criterion and Griffith criterion. The later is based on a critical value G_c of the energy release rate G defined as the derivative of the potential energy with respect to the crack length (Griffith, 1921).

Recently, failure laws for two-dimensional domains with V-notches, multi-material interfaces or orthotropic materials have attracted major interest because of the relation to composite materials and electronic devices. A sufficiently simple and reliable condition for predicting failure initiation (crack formation) in the above mentioned cases, involving singular points, is still a topic of active research and interest. At such points the stress tensor is infinity under the assumption of linear elasticity. A typical example of a singular point is the reentrant V-notch tip, for which a crack tip is a particular case when the V-notch opening angle is of zero degrees.

For these general singular points, namely, singularities associated with corners, non-isotropic multi-material interfaces and abrupt changes in boundary conditions, the linear elastic displacements field in the vicinity of the singular point is expressed by:

$$\mathbf{u} = \sum_{\ell=1}^{L} \sum_{m=0}^{M} A_{\ell,m}\, r^{\alpha_\ell} \ln^m r \left\{ \begin{array}{c} u_1^{(\ell,m)}(\theta) \\ u_2^{(\ell,m)}(\theta) \end{array} \right\} + \mathbf{u}_{\text{reg}}, \tag{2}$$

where α_ℓ (denoted by eigen-values) may be any number greater than zero, or complex numbers with the real part greater than zero and under special circumstances, where $m \neq 0$, power-logarithmic stress singularity may exist (as shown in (Dempsey, 1995) these singularities typically occur on transition loci separating regions of real and complex eigen-values). These cases when power-logarithmic stress singularities exist are not addressed herein, and in this case we consider expression (1).

In the aforementioned, to our best knowledge, a small volume of research activity has been conducted in the past for establishing a failure law applicable to brittle materials. The works of Dunn et al. (1997a, b) provide experimental correlation of A_1 (and possibly A_2) to fracture initiation in the case that α_1 and α_2 are real and the singular points are V-notches in isotropic materials. Hattori et al. (1989, 1991) propose a two-parameter failure law based on A_1 and the exponent α_1 for V-notch configurations, and demonstrated that a good correlation is achieved with experimental results. Reedy and Guess (1995, and the references therein), correlated failures of adhesive-bonded butt tensile joints with A_1. In all these cases a V-notch configuration is addressed, and no special attention is devoted to the connection of A_ℓ, α_ℓ and $\mathbf{u}^{(\ell)}(\theta)$. Novozhilov (1969) proposed a simple failure criterion based on the average normal stress along the anticipated path of the crack formation. The validity of Novozhilov criterion has been examined by Seweryn (1994) by experiments performed on V-notch samples. Leguillon (2001, 2002) proposed a criterion for failure initiation at a sharp V-notch based on a combination of the Griffith energy criterion for a crack, and the strength criterion for a straight edge. This approach provides a criterion similar to Novozhilov criterion, and shows good agreement with experimental observations in Dunn et al. (1997b). A very recent work by Seweryn and Lukaszewicz (2002) addresses some of the failure criteria in the vicinity of a V-notch tip under mixed mode loading. Herein, we examine two of the most promising failure criteria (and discuss them in more detail in the sequel), the one proposed by Leguillon based on the strain energy release rate, and the second based on averaged stress by Novoshilov–Seweryn, and suggest a simplified failure criteria based on the strain energy density. This criterion was presented in Amar and Yosibash (2002), denoted as the SED criterion. It proposes as the failure criterion the critical value of the average strain energy in a sector in the vicinity of the singular point over the volume of this sector. Same criterion has been also studied by Lazzarin and Zambardi (2001), denoted in their paper as the 'finite-volume-energy' criterion, and good correlation to experimental data of other publications is demonstrated. The SED is

rigourously treated herein from the mathematical point of view, bringing its formulation to a contour integral using the expansion in (1), and validated by our own experiments. Although we denote this failure criterion as the SED criterion, it is a different criterion as the SED criterion by Sih (see, e.g. Sih and Macdonald, 1974), as will be explained in Section 2.

Cases when α_1 is complex are not addressed either. Some possible definition of complex stress intensity factors associated with interface cracks (when α_1 is complex) are given by Rice (1988) and Suo (1989). The complex representation of the displacements field in the neighborhood of a general two-dimensional singular point poses several difficulties in establishing a failure law. Therefore, it is desirable that any proposed failure criterion has the following properties:

(a) Independent of the units used. I.e., given the criterion for two different opening angles (ω_1 and ω_2), in a unit system, let us say F_1 and F_2, then a change of units must not change the ratio F_1/F_2.
(b) Uniquely applicable to real and complex eigen-values (as in the case of cracks in a bi-material interface).
(c) Uniquely applicable to single and mixed mode loading.
(d) Degenerate to known failure criteria for cracks when reentrant V-notch angle is zero, and to strength criteria for straight edge (V-notch angle of 180°).

As in reality no V-notch tip is sharp, but has a rounded (finite) tip, so our purpose is to examine quantitatively the influence of the V-notch tip radius on failure initiation. We perform a parametric examination on the deviation of the predicted values (by the failure laws, assuming a sharp tip) compared to experimental observations.

The paper is organized as follows: We start with notations and a short description of the functional representation of the solution in the neighborhood of a singular point. Then review three published failure initiation criteria, compare between them, including their advantages and drawbacks. In Section 2 we formulate and discuss in details the 'Strain Energy Density' (SED) failure criterion. The validity of the various criteria is investigated by comparison to experimental observations. Sets of experiments performed on composite ceramic Alumina-7%Zirconia, and Poly-Methyl-Methacrylate (PMMA, or known as Plexiglass) V-notched specimens are summarized in Section 3. These mimic 2-D domains under plane-strain condition, made of brittle materials, and loaded so as to produce 'mode I' stress field in the neighborhood of the singular point. The necessary information for the various failure criteria is extracted from p-finite element analysis simulating the experimental data, and documented in Section 4. Using the extracted information, the validity of the various failure laws in predicting the experimental observations is investigated. Finally, conclusions are given in Section 5.

1.1. Singular solutions and notations

Consider a 2-D domain having a V-notch reentrant corner as described in Figure 1, assuming that the V-notch tip is sharp, i.e. $\rho = 0$ (this assumption will be removed in the sequel). By locating a cylindrical coordinate system in the V-notch tip, the displacements and stresses in the vicinity of the singular point are represented by the asymptotic series (1) so the stresses are given by :

$$\boldsymbol{\sigma} = \sum_{\ell=1}^{L} A_\ell \, r^{\alpha_\ell - 1} \begin{Bmatrix} s_{11}^{(\ell)}(\theta) \\ s_{22}^{(\ell)}(\theta) \\ s_{12}^{(\ell)}(\theta) \end{Bmatrix} + \boldsymbol{\sigma}_{\text{reg}} = \sum_{\ell=1}^{L} A_\ell r^{\alpha_\ell - 1} \mathbf{s}^{(\ell)}(\theta) + \boldsymbol{\sigma}_{\text{reg}}, \tag{3}$$

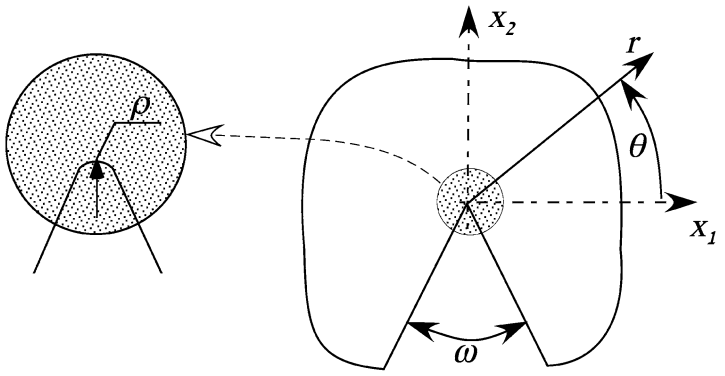

Figure 1. The singular point and notations.

where A_ℓ's depend on the loading and boundary conditions away from the singular point, directions 1 and 2 mean x_1 and x_2, and $\boldsymbol{\sigma}_{\text{reg}}$ is a regular stress tensor, remaining bounded as r tends to zero. The eigen-pairs $\alpha_\ell (\leq \alpha_{\ell+1})$ and $\mathbf{u}^{(\ell)}(\theta)$ depend on the geometry, boundary conditions and material properties in the vicinity of the singular point.

These eigen-pairs may be complex, in which case they appear in pairs of a complex number and its conjugate. For example, assume the first eigen-pair is a complex number, i.e. $\alpha_1 = \alpha_1^{\Re} + \imath\alpha_1^{\Im}$ and $\mathbf{s}^{(1)}(\theta) = \mathbf{s}^{(1),\Re} + \imath\mathbf{s}^{(1),\Im}$, so that $\alpha_2 = \alpha_1^{\Re} - \imath\alpha_1^{\Im}$ and $\mathbf{s}^{(2)}(\theta) = \mathbf{s}^{(1),\Re} - \imath\mathbf{s}^{(1),\Im}$ ($\imath \overset{\text{def}}{=} \sqrt{-1}$). In this case, it is common to express the associated generalized stress intensity factors as a complex number $A_1 + \imath A_2$ and its conjugate $A_1 - \imath A_2$. Denoting $\delta = \alpha_1^{\Im} \ln(r)$, the stresses in series (1) take the form:

$$\begin{aligned}
\sigma_{jk} &= (A_1 + \imath A_2) r^{\alpha_1^{\Re} - 1 + \imath\alpha_1^{\Im}} (s_{jk}^{(1),\Re}(\theta) + \imath s_{jk}^{(1),\Im}(\theta)) \\
&\quad + (A_1 - \imath A_2) r^{\alpha_1^{\Re} - 1 - \imath\alpha_1^{\Im}} (s_{jk}^{(1),\Re}(\theta) - \imath s_{jk}^{(1),\Im}(\theta)) + \textstyle\sum_{\ell=3}^{L} A_\ell \, r^{\alpha_\ell - 1} s_{jk}^{(\ell)}(\theta) + (\sigma_{jk})_{\text{reg}}. \\
&= A_1 r^{\alpha_1^{\Re} - 1} \left[2(s_{jk}^{(1),\Re}(\theta) \cos\delta - s_{jk}^{(1),\Im}(\theta) \sin\delta) \right] \\
&\quad + A_2 r^{\alpha_1^{\Re} - 1} \left[-2(s_{jk}^{(1),\Re}(\theta) \sin\delta + s_{jk}^{(1),\Im}(\theta) \cos\delta) \right] + \textstyle\sum_{\ell=3}^{L} A_\ell \, r^{\alpha_\ell - 1} s_{jk}^{(\ell)}(\theta) + (\sigma_{jk})_{\text{reg}}.
\end{aligned} \tag{4}$$

Although some of the failure criteria can be generalized to these cases involving complex eigen-pairs (like the Leguillon criterion and the SED criterion in the sequel), these are not addressed herein.

There may be also situations for which power logarithmic singularities exist, i.e. terms of the form $r^{\alpha_\ell} \log r$ (see e.g. Dempsey, 1995), cases which will not be addressed herein either.

1.2. Novozhilov–Seweryn criterion

The failure criterion proposed by Novozhilov (1969) and expanded by Seweryn (1994), suggests to consider the average normal stress along the anticipated path of the failure. So failure occurs when the average stress equals a material dependent value, denoted by σ_c, which is the stress at failure without the presence of a notch. A characteristic length scale is introduced, denoted by d_0, along which the average stress is considered. Let us assume that the failure will occur along axis x_2 in Figure 1. Based on (1), the average normal stress to axis x_2 is σ_{11}. Integrating along a distance d_0, the average stress is defined by:

$$\begin{aligned}\sigma_c &= \frac{1}{d_0}\int_0^{d_0}\sum_{\ell=1}^{L} A_\ell\, r^{\alpha_\ell} s_{11}^{(\ell)}(\theta = 90^\circ)\,\mathrm{d}x_2 \\ &= \sum_{\ell=1}^{L}\frac{A_\ell}{\alpha_\ell} d_0^{\alpha_\ell - 1}\, s_{11}^{(\ell)}(\theta = 90^\circ).\end{aligned} \tag{5}$$

Assume that $d_0 \ll 1$, then all terms for $\ell \geq 2$ are negligible in comparison with the first term in the series, so that (1) simplifies to:

$$\sigma_c = \frac{A_1}{\alpha_1} d_0^{\alpha_1 - 1}\, s_{11}^{(1)}(\theta = 90^\circ). \tag{6}$$

For the well-known particular case of a crack, failure occurs when

$$A_1 s_{11}^{(1)}(\theta = 90^\circ) = \frac{K_{I_c}}{\sqrt{2\pi}}, \tag{7}$$

where K_{I_c} is the plane strain fracture toughness. Eliminating A_1 from (7), and substituting $\alpha_1 = 1/2$ in (6), one obtains:

$$d_0 = \frac{2}{\pi}\frac{K_{I_c}^2}{\sigma_c^2}. \tag{8}$$

Coming back to (6), and substituting d_0 from (8) we finally obtain:

$$A_1 s_{11}^{(1)}(\theta = 90^\circ) = \alpha_1 \sigma_c \left(\frac{2}{\sqrt{2\pi}}\frac{K_{I_c}}{\sigma_c}\right)^{2-2\alpha_1}. \tag{9}$$

In the sequel, the value $A_1 s_{11}^{(1)}(\theta = 90^\circ)$ is called generalized stress intensity factor (GSIF), and its value at failure is denoted by $k_c \stackrel{\text{def}}{=} \text{GSIF}_{cr}$.

The above criterion proposed by Novozhilov (1969) has the advantage of reducing to the well known classical failure criterion for cracks, when $\alpha_1 = 1/2$:

$$A_1 s_{11}^{(1)}(\theta = 90^\circ) = \frac{K_{I_c}}{\sqrt{2\pi}}$$

and the usual strength criterion for a straight edge (when $\omega = \pi$, so that $\alpha_1 = 1$):

$$A_1 s_{11}^{(1)}(\theta = 90^\circ) = \sigma_c$$

Seweryn (1994) examined the validity of Novozhilov's failure criterion by performing experiments on V-notch samples made of plexiglass and Dualuminum having opening angle of $\omega = 20^\circ$ to 180°, with tip radius of $\rho = 0.01$ mm. Using the critical load at failure, the generalized stress intensity factor at failure can be computed, and by using (9) one can predict the fracture toughness:

$$K_{I_c} = \frac{\sqrt{2\pi}\sigma_c}{2}\left(\frac{A_1 s_{11}^{(1)}(\theta = 90^\circ)}{\alpha_1 \sigma_c}\right)^{\frac{1}{2-2\alpha_1}}. \tag{10}$$

Because the K_{I_c} value is not known, it has been computed from the results obtained for the various opening angles. Table 1 summarizes the results reported by Seweryn (1994).

Table 1. Values of $(2\pi)^{1-\alpha}A_1 s_{11}^{(1)}(\theta = 90°)$ [MPa $\mathrm{m}^{1-\alpha}$] and K_{I_c} [MPa $\sqrt{m}$] computed by (10) from Seweryn (1994)

ω	20°	40°	60°	80°	100°	120°	140°	160°
Plexiglass								
Computed K_{I_c}	1.859	1.789	1.960	1.892	1.752	1.561	1.594	2.493
$(2\pi)^{1-\alpha}A_1 s_{11}^{(1)}(\theta = 90°)$	1.866	1.851	2.167	2.436	3.059	4.347	8.861	28.60
Duraluminum								
Computed K_{I_c}	53.39	55.85	56.67	56.24	56.10	53.40	49.62	53.18
$(2\pi)^{1-\alpha}A_1 s_{11}^{(1)}(\theta = 90°)$	53.51	57.10	60.53	66.34	80.15	102.00	150.44	291.81

As can be noticed in Table 1, as the opening angle ω increases, the criterion's validity deteriorates. Very recently, the Novoshilov–Seweryn failure criterion has been extended to mixed mode failure by Seweryn and Lukaszewicz (2002), where its validity compared to other failure criteria in predicting the failure load and direction is demonstrated when compared to experimental observations.

1.3. Leguillon criterion

Leguillon (2001, 2002) proposed a criterion for failure initiation at a sharp V-notch based on a combination of the Griffith energy criterion for a crack, and the strength criterion for a straight edge. This approach is based on the change of the potential energy in a notched specimen due to a creation of a small crack in the direction θ_0 which generates maximum change in potential energy. Here as well, a characteristic length scale is introduced, which is the length of the created crack ℓ_0:

$$\ell_0 = \frac{\left(s_{\theta\theta}^{(1)}(\theta_0)\right)^2}{K(\omega)} \frac{K_{I_c}^2}{\sigma_c^2}. \tag{11}$$

For a V-notch in an isotropic material under symmetrical loading, the *critical material dependent parameter* k_c is given by:

$$k_c \overset{\text{def}}{=} A_1 s_{11}^{(1)}(\theta = 90°) = \left(\frac{G_c}{K(\omega)}\right)^{1-\alpha_1} \sigma_c^{2\alpha_1 - 1}, \tag{12}$$

where G_c is the fracture energy per a unit surface (also denoted by *toughness*) and σ_c is the 1-D stress at brittle failure (*strength*), both being material properties. The parameter $K(\omega)$ depends on the local geometry and boundary conditions in the neighborhood of the V-notch tip, the eigen-value α and its corresponding eigen-function, and the material properties (E and ν in isotropic materials) . It is important to realize that $K(\omega)$ is not the generalized stress intensity factor for the V-notch, but is computed by an integration procedure as shown in the appendix of (Leguillon, 2002). For example, in Table 2 by Leguillon (2002), the values of $K(\omega)$ for a V-notch in PMMA which is an isotropic homogeneous material with $E = 2.3$ GPa and $\nu = 0.36$ are given, see Table 2.

Based on Table 2 and the expression for evaluating $K(\omega)$, for any traction free reentrant V-notch configuration in an isotropic homogeneous material with new material properties E^{new} and ν^{new} the new values of $K(\omega)$ may be easily obtained:

Table 2. Values of $K(\omega)$ as reported by Leguillon (2002)

ω	0°	30°	45°	60°	90°	120°	150°	165°	180°
$K(\omega)$	0.00248	0.00243	0.00242	0.00237	0.00212	0.00176	0.00128	0.00098	0.00069

Table 3. Values of $K(\omega)$ for Alumina-7%Zirconia

ω	30°	60°	90°	120°
$K(\omega)$	1.68683E-05	1.64518E-05	1.47164E-05	1.22174E-05

$$K^{\text{new}}(\omega) = K(\omega)\frac{2.3}{1-0.36^2}\frac{1-(\nu^{\text{new}})^2}{E^{\text{new}}}, \qquad E^{\text{new}} \quad \text{in GPa} \tag{13}$$

For example for Alumina-7%Zirconia with $E \approx 360$ GPa and $\nu = 0.23$, the new values for $K(\omega)$ are given in Table 3.

Correlation of the current criterion with experimental observations in PMMA V-notched specimens as well as in bi-material wedges shows a good agreement.

1.4. Dunn et al. criterion

Dunn et al. (1997b) proposed to use the V-notch generalized stress intensity factor (GSIF), denoted by k_c as the single parameter to be correlated to failures. k_c values were obtained at failure by using experiments done on PMMA specimens (Dunn et al., 1997b) and single crystal Silicon (Suwito and Dunn, 1998) show reasonable similarity for sharp V-notch angles. This method requires the evaluation of k_c for each V-notch opening angle. Furthermore, its applicability for large opening angle is questionable (as $\omega \to \pi$, approaching a straight edge, the eigen-stresses tend to be a constant, thus the generalized stress intensity factor is meaningless).

Although the addressed criteria provide good correlation to experimental observations, there are some difficulties in applying them because:

(1) The units of the critical 'stress intensity factor' are somewhat entangled.

(2) It is difficult to generalize the methods to a mixed mode loading.

(3) The critical stress intensity factor (K_{Ic}) for the material of interest has to be known.

(4) A fracture stress σ_c has to be assumed. This value may be taken as σ_Y (yield stress), and for brittle materials it is *supposed* to be also the stress at fracture. However, even for brittle materials, the stress at fracture is higher than the conventional definition of σ_Y.

To overcome these difficulties, and provide a simpler failure criterion, we suggest the use of a simpler concept in the next section.

2. The strain energy density (SED) criterion

It is conceivable to assume that failure initiates when the average elastic strain energy contained in a sector having the singular point as its center, over the volume of this sector, reaches a critical value. This averaged elastic strain energy density, which we denote by strain energy

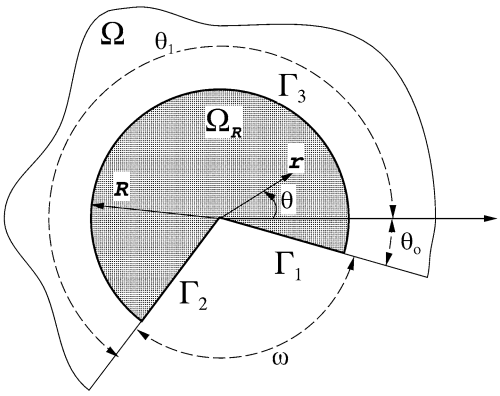

Figure 2. The SED domain of interest and notations.

density (SED), and Lazzarin and Zambardi (2001) denote by finite-volume-energy, reminds the well known SED criterion by Sih and Macdonald (1974). However these are considerably different in several respects. The SED of Sih is a *pointwise value* evaluated at any point on an arc located at a radius R away from the crack tip and is usually applied to crack tip singularities. Because it is a function of θ, a minimum value of Sih's SED can be found at a given angle θ^*. Thus, Sih's SED may be used as a criterion for predicting the crack propagation direction, as well as a failure criterion. This pointwise minimum, correlated to a critical material dependent parameter, is the failure criterion. The SED failure criterion proposed herein is an *avaraged value*, is not aimed at predicting directions of crack propagation, but at predicting failure initiation at a specific critical value independent of the opening angle of the V-notch tip.

Consider a circular sector Ω_R of radius R centered in the singular point:

$$\Omega_R \stackrel{\text{def}}{=} \{(r,\theta) | 0 \le r \le R,\ \theta_0 \le \theta \le \theta_1\},$$

with traction free boundary conditions on the faces intersecting in the singular point. See Figure 2.

The elastic strain energy $\mathcal{U}(\mathbf{u})[R]$ in a 2-D domain of constant thickness b under the assumption of plane-strain is defined as:

$$\mathcal{U}(\mathbf{u})[R] \stackrel{\text{def}}{=} \tfrac{1}{2} b \iint_{\Omega_R} \sigma_{jk}\varepsilon_{jk}\, \mathrm{d}\Omega \qquad j,k = 1,2, \tag{14}$$

where summation notation is implied unless otherwise specified. Using the kinematic connections between strains and displacements $\varepsilon_{jk} = \frac{1}{2}(\partial_j u_k + \partial_k u_j)$, then using Green's theorem we transform the area integral in (14) into a boundary integral on $\partial\Omega_R$:

$$\mathcal{U}(\mathbf{u})[R] = \tfrac{1}{2} b \int_{\partial\Omega_R} \sigma_{jk} n_k u_j\, \mathrm{d}S, \tag{15}$$

here n_j is the jth component of the outward normal vector to the boundary $\partial\Omega_R$. Along the two straight lines Γ_1 and Γ_2 this integral is zero because of the traction free boundary conditions. Reuse the strain-stress connection, we finally express the strain energy in Ω_R by a 1-D integral:

$$\mathcal{U}(\mathbf{u})[R] = \tfrac{1}{2} b \int_{\theta_0}^{\theta_1} \left[\sigma_{jk} n_k u_j\right]_{r=R} R\, \mathrm{d}\theta. \tag{16}$$

Note that on Γ_3 the outward normal vector is $(\cos\theta,\ \sin\theta)$, and using (1), (16) becomes:

$$\mathcal{U}(\mathbf{u})[R]= \tfrac{1}{2}b\sum_{k,\ell}A_kA_\ell R^{\alpha_k+\alpha_\ell}\int_{\theta_0}^{\theta_1}\Big[s_{11}^{(k)}(\theta)u_1^{(\ell)}(\theta)\cos\theta+s_{12}^{(k)}(\theta)\Big(u_1^{(\ell)}(\theta)\sin\theta+u_2^{(\ell)}(\theta)\cos\theta\Big) +s_{22}^{(k)}(\theta)u_2^{(\ell)}(\theta)\sin\theta\Big]\,\mathrm{d}\theta \tag{17}$$

For isotropic materials, with traction free boundary conditions in the neighborhood of the singular point, the following orthogonality rule holds (see e.g. Yoshibash, 1994):

$$\int_{\theta_0}^{\theta_1}\Big[s_{11}^{(k)}u_1^{(\ell)}\ \cos\theta+s_{12}^{(k)}\Big(u_1^{(\ell)}\ \sin\theta+u_2^{(\ell)}\ \cos\theta\Big)+s_{22}^{(k)}u_2^{(\ell)}\ \sin\theta\Big]\,\mathrm{d}\theta=0\quad\text{for}\quad k\neq\ell, \tag{18}$$

which simplifies (17) to:

$$\mathcal{U}(\mathbf{u})[R]=\tfrac{1}{2}\sum_{k}A_k^2R^{2\alpha_k}\int_{\theta_0}^{\theta_1}\Big[s_{11}^{(k)}u_1^{(k)}\cos\theta+s_{12}^{(k)}\Big(u_1^{(k)}\sin\theta+u_2^{(k)}\cos\theta\Big)+s_{22}^{(k)}u_2^{(k)}\sin\theta\Big]\,\mathrm{d}\theta. \tag{19}$$

We define the strain energy density (SED) as:

$$\mathrm{SED}[R]\overset{\mathrm{def}}{=}\frac{\mathcal{U}(\mathbf{u})[R]}{b\times\Omega_R}$$

so, using (19), we finally obtain:

$$\mathrm{SED}[R]=\ \frac{1}{2\pi-\omega}\sum_{k}A_k^2R^{2\alpha_k-2}\int_{\theta_0}^{\theta_1}\Big[s_{11}^{(k)}u_1^{(k)}\cos\theta+s_{12}^{(k)}\Big(u_1^{(k)}\sin\theta+u_2^{(k)}\cos\theta\Big) +s_{22}^{(k)}u_2^{(k)}\sin\theta\Big]\,\mathrm{d}\theta. \tag{20}$$

The SED$[R]$, depends of course on a typical length size R, and it should be small enough so that Ω_R is within the K-dominance region, ensuring that the singular terms represent the exact solution. To ensure that this holds, $\mathcal{U}(\mathbf{u})[R]$ is computed first by using (19), followed by a second computation using the stress and strain tensors according to (14). If the two computations provide different results, the domain Ω_R is too large, and only one term in the asymptotic expansion does not represent well the stress field within the sector of radius R. On the other hand, R should be large enough so it is larger compared to the plastic radius r_p and the V-notch tip radius ρ.

Of course, the value of SED$[R]$ has to be in the range of the two extremes obtained for $\omega=0^\circ$ (a crack) and $\omega=180^\circ$ (a straight edge). The expressions for $\mathrm{SED}[R]_{\mathrm{straight}}$ and $\mathrm{SED}[R]_{\mathrm{crack}}$ in terms of K_{Ic} and σ_c are given in Appendix A, and as will be shown for the two brittle materials used in our investigation $\mathrm{SED}[R]_{\mathrm{straight}}\approx\mathrm{SED}[R]\approx\mathrm{SED}[R]_{\mathrm{crack}}$ when R is chosen properly. As will be shown in the sequel, for brittle materials, the upper and lower restrictions on R can be met. Also, using K_{Ic} and σ_c, one can compute a material dependent integration radius R_{mat}, so that the SED is independent of the opening angle ω (see derivation in Appendix A), obtaining:

$$R_{\mathrm{mat}}=\frac{(1+\nu)(5-8\nu)}{4\pi}\left(\frac{K_{Ic}}{\sigma_c}\right)^2. \tag{21}$$

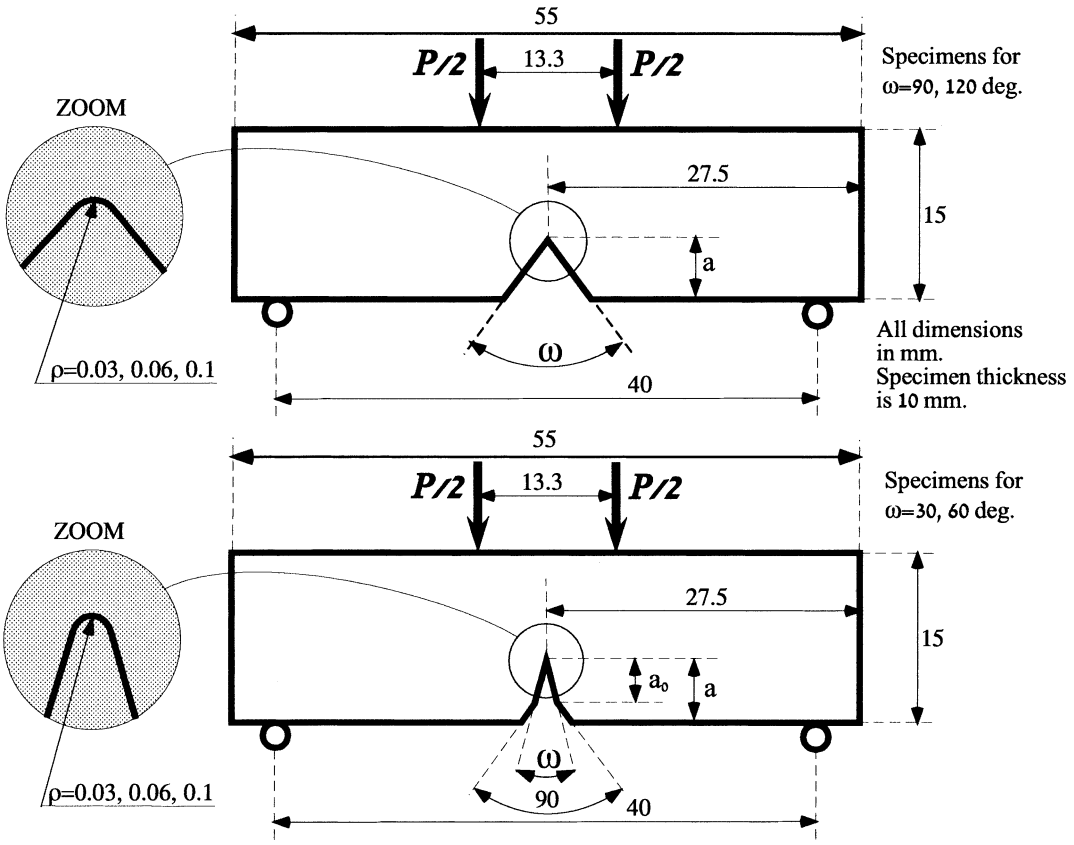

Figure 3. Specimen geometry and loading configuration (FPB type) for the Alumina-7%Zirconia case.

However, this integration radius R_{mat} may be required to be smaller in size compared to the plastic radius or the V-notch tip radius ρ, or larger than the K-dominance zone. In this case, given the value of SED$[R_1]$, one can easily determine the value of SED for a domain having a different radius R_2 by the simple equation derived from (20):

$$\text{SED}[R_2] = \text{SED}[R_1]\left(\frac{R_1}{R_2}\right)^{2-2\alpha_1}. \tag{22}$$

3. Materials and experimental procedures

The validity of the various failure criteria has to be assessed combined with a set of experimental data. This section presents a series of experiments which has been performed on two kinds of brittle materials: the composite ceramic Alumina-7%Zirconia and the polymer PMMA, both having a linear elastic constitutive law. The tests have been carried out on V-notched specimens loaded by three-points and four-points bending. The determination of the mechanical and physical properties of tested materials as well as the exact details of the experimental procedures and characterization techniques utilized will be reported elsewhere.

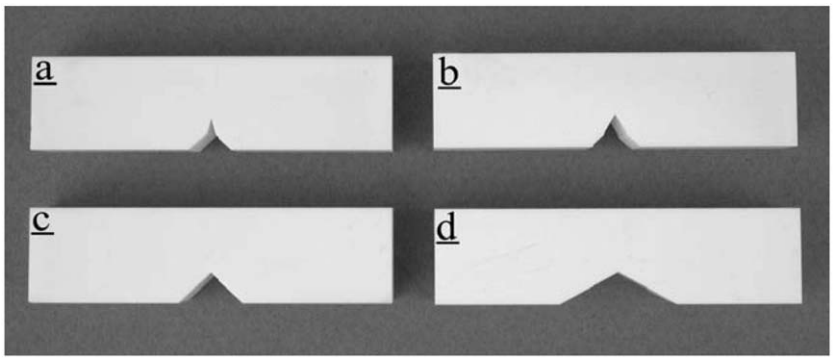

Figure 4. Alumina-7%Zirconia specimens with various radii and notch angles; (a) 0.06 mm, 30° (b) 0.1 mm, 60° (c) 0.1 mm, 90° (d) 0.1 mm, 120°.

3.1. Experiments with Alumina-7%Zirconia

First set of experiments is performed on V-notched specimens under a tight control of the geometric dimensions (including the V-notch tip radius ρ). Over 70 specimens were manufactured with four V-notch opening angles $\omega = 30°, 60°, 90°$ and 120°, each having three different tip radii $\rho = 0.03, 0.06$ and 0.1 mm. The specimens were loaded so to produce pure 'symmetric mode' stress field in the vicinity of the V-notch tip. The geometry and the loading of the various Alumina-7%Zirconia specimens are presented in Figure 3. TPB (three point bending) loading was also applied to some of the specimens where a single load was applied opposite to the V-Notch tip. The notch depth a was approximately 5 mm, and varies slightly from specimen to specimen, and $a_o \approx 2.5$ mm for the specimens with the double opening angles $\omega = 30°, 60°$. The precise dimensions for each specimen have been measured and used later on for the computations. Some representative specimens with various V-notch opening angles are shown in Figure 4.

Physical properties, Young modulus E, and Poisson ratio ν have been accurately measured using ultra-sonic technique, while density has been determined by actual measurements of mass and volume. Table 4 summarizes the values measured on a sample of the specimens obtaining $\nu = 0.236$ with minor changes in the third digit.

We used the values of 357 or 350 GPa as the Young modulus (the value of 350 GPa has been assigned to the specimens for which we did not measured their material properties according to the value reported in literature) with $\nu = 0.236$ in our analysis in Section 4.

The specimens were subject to a quasi-static loading (crosshead velocity was 0.5 mm min^{-1}) using a computerized MTS servo-hydraulic machine, with sensitive load cell of 1-ton full scale. V-notch opening displacement was measured by a crack opening displacement (COD) gage (full scale of 0.25 mm), which was mounted at the V-notch intersection with the free edge. In microscopic scale, acoustic emission (AE) technique was used in order to monitor events during loading from undesired sources. It enables to point out on inhomogeneity in the microstructure such as; high porosity/microcracks/impurities, thus provide the means in excluding specimens with abnormal behavior (intense AE activity). The experimental set-up including the AE sensor is illustrated in Figure 5.

Examples of load vis. displacement behavior obtained for typical specimens are shown in Figure 6. Specimens which exhibited linear elastic response are illustrated by Figure 6a, while specimens with non-linear load-displacement characterized by slow crack growth, smooth and

Table 4. Measured E, density and ν for selected specimens

Specimen	E (GPa)	Density (g/cm^3)	ν
30-FPB-0.1-1	356.52	3.963	0.235
30-FPB-0.1-2	356.89	3.965	0.236
30-FPB-0.1-3	355.30	3.962	0.233
30-TPB-0.1-4	357.90	3.970	0.235
30-FPB-0.03-4	360.24	3.975	0.239
30-FPB-0.03-5	359.85	3.975	0.236
30-FPB-0.03-6	357.31	3.976	0.233
60-FPB-0.1-1	354.00	3.963	0.235
60-FPB-0.1-2	367.31	3.965	0.238
60-FPB-0.1-3	369.53	3.962	0.238
60-FPB-0.1-4	355.20	3.970	0.235
60-FPB-0.03-2	357.71	3.964	0.238
60-FPB-0.03-3	356.50	3.968	0.234
90-FPB-0.1-5	355.50	3.956	0.235
90-FPB-0.1-6	358.70	3.958	0.235
90-FPB-0.1-7	356.06	3.951	0.235
90-FPB-0.03-3	354.50	3.959	0.239
90-FPB-0.03-4	355.40	3.959	0.239
90-FPB-0.03-5	338.50	3.898	0.235
90-FPB-0.03-6	349.70	3.940	0.238
Average	356.63	3.960	0.236

non continuous one are depicted in Figures 6b and 6c respectively. A case where intense AE activity is pronounced in the later stage of loading is shown in Figure 6d. Specimens which exhibited nonlinear load-displacement behavior, also had large acoustic emission counts prior to failure, evidently due to impurities and microcracks. These specimens were excluded.

Details of V-notch angle and tip radius were documented optically for each specimen before and after fracture, as shown in Figure 7. This systematic procedure was done in order to eliminate specimens with macroscopic defects due to manufacturing problems (irregularities and non-symmetry at the notch radius). In addition, cracks, which were originated far away from the notch root were also discarded from calculations, see such an example in Figure 8a. In comparison, crack which initiated close to the notch root is shown in Figure 8b.

For the remaining specimens ('good results') the values of the notch tip radius ρ, the fracture load P and Young modulus E are listed in Table 5. The last four columns in the tables are computed values addressed in the next section. Specimens denoted by 'TPB' were loaded in three point bending mode, at the middle of the span.

In Appendix B we provide the full list of all tested specimens.

3.2. Experiments with PMMA

Dunn et al. (1997b) carried out a set of experiments on notched PMMA specimens loaded by three-point bending, with notch angles of 60°, 90° and 120° for various V-notched depths

Table 5. Summary of the experiments for the 'good Alumina-7%Zirconia specimens', and GSIFs (k_c)

Specimen	ρ	P	E	SED (0.062 mm)	$A_1 s_{11}^{(1)}(90°)$ computed by (12)	$A_1 s_{11}^{(1)}(90°)$ computed by (9)	$(A_1)_{cr} s_{11}^{(1)}(90°)$ experiments
	mm	N	GPa	$\frac{\text{N}}{\text{m}^2}$		MPa $\times$ $\text{m}^{1-\alpha_1}$	
$\omega = 30°, \alpha_1 = 0.501453$							
AO30003-16	0.031	1815	350	173547	1.643	1.662	1.942
30-TPB-0.03-3	0.040	1436	350	164253	1.643	1.662	1.863
AO30003-11	0.041	1628	350	137811	1.643	1.662	1.732
AO30006-13	0.060	1628	350	140944	1.643	1.662	1.751
30-TPB-0.1-4	0.060	1439	356.7	127912	1.627	1.662	1.690
30-TPB-0.1-5	0.060	1413	350	103800	1.643	1.662	1.509
AO3001-12	0.100	1844	350	179506	1.643	1.662	1.976
$\omega = 60°, \alpha_1 = 0.512221$							
15.4.02 - 11	0.060	1753	350	155625	1.859	1.870	2.010
15.4.02 - 12	0.060	1701	350	148996	1.859	1.870	1.967
15.4.02 - 15	0.060	1603	350	128253	1.859	1.870	1.826
15.4.02 - 18	0.060	1680	350	137102	1.859	1.870	1.888
A06001-12	0.100	1785	350	168763	1.859	1.870	2.095
A06001-13	0.100	1903	350	196644	1.859	1.870	2.262
$\omega = 90°, \alpha_1 = 0.5444837$							
90-FPB-0.03-5	0.035	1853	338.5	164962	2.774	2.655	2.844
90-TPB-0.03-7	0.050	1292	350	132235	2.732	2.655	2.596
90-TPB-0.06-1	0.060	1523	350	158707	2.732	2.655	2.842
90-TPB-0.06-2	0.060	1642	350	184986	2.732	2.655	3.071
90-TPB-0.06-3	0.067	1461	350	145375	2.732	2.655	2.722
90-FPB-0.1-5	0.100	2167	356.7	183066	2.708	2.655	3.077
90-FPB-0.1-6	0.100	2244	356.7	198267	2.708	2.655	3.201
90-TPB-0.1-3	0.100	1724	350	197814	2.732	2.655	3.176
$\omega = 120°, \alpha_1 = 0.6157311$							
120-TPB-0.03-5	0.062	1962	350	171724	6.087	5.688	6.329
120-TPB-0.06-1	0.080	1927	350	175779	6.087	5.688	6.403
120-TPB-0.06-2	0.080	1805	350	157698	6.087	5.688	6.065
120-TPB-0.06-3	0.080	1958	350	178687	6.087	5.688	6.456
120-FPB-0.1-3	0.100	2928	350	255128	6.087	5.688	7.705
120-FPB-0.1-5	0.100	2892	350	265188	6.087	5.688	7.853
120-TPB-0.1-6	0.100	2053	350	236806	6.087	5.688	7.435

Figure 5. Four-point-bending test fixture with acoustic emission transducer and crack opening displacement gage (PMMA specimen).

(a/h from 0.1 to 0.4), and V-notch tip radius of less than 0.0254 mm. The material properties of the PMMA are $E = 2.3$ GPa and $\nu = 0.36$, with the failure stress being $\sigma_c = 124$ MPa. The failure load values are summarized in Tables 6 and 7 in the first column. These loads are for different V-notch depths, but using the load at failure and specific geometrical dimensions, the GSIF at failure is computed and reported in the last column of the tables. No results for the angle of $\omega = 45^\circ$ are reported by Dunn et al. (1997b). Here, similar specimens were manufactured with $a/h = 0.235$, and V-notch tip radius of 0.03 mm, which were loaded up to fracture in TPB. The results are reported in the first two rows of Table 6.

4. Verification and validation of the failure criteria

In order to validate the various failure criteria, we constructed finite element models of the various specimens tested, and loaded these by the load that caused the fracture. The p-FEM (Szabó and Babuška, 1991) commercial code StressCheck[1] has been used in our computations. An example of the FE mesh for a $\omega = 90^\circ$ case and the zoomed portion in the neighborhood of the notch tip is shown in Figure 9.

The special optimal mesh design using geometric progression of the elements with a factor of 0.17 towards the singular point ensures high accuracy and exponential convergence rates in the pre-asymptotic range. The polynomial degree has been increased over each element from 1 to 8, and the numerical error measured in energy norm (see, e.g., Szabó and Babuška, 1991) is monitored. As a post solution operation, we extract the eigen-pairs $(\alpha_\ell, \mathbf{u}^{(\ell)}(\theta))$ associated

[1]StressCheck is trademark of Engineering Software Research and Development, Inc, St. Louis, MO, USA.

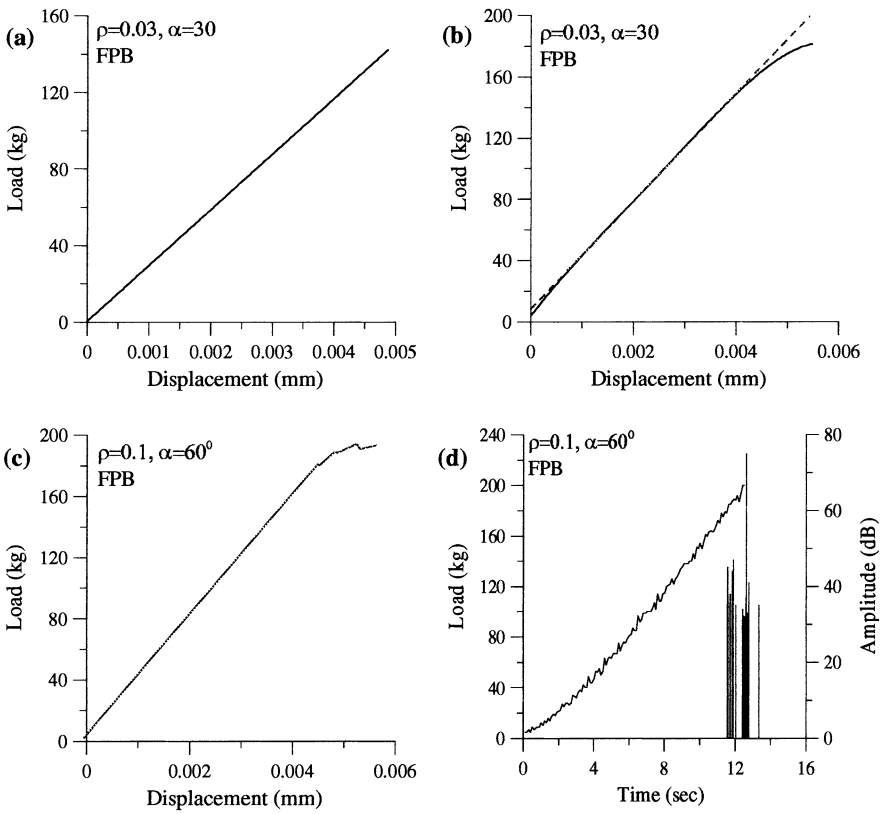

Figure 6. Load-Displacement curves for linear-elastic behavior (a) and non-linear response (b, c). (d) shows load and acoustic emission amplitude vs. time for the (c) case.

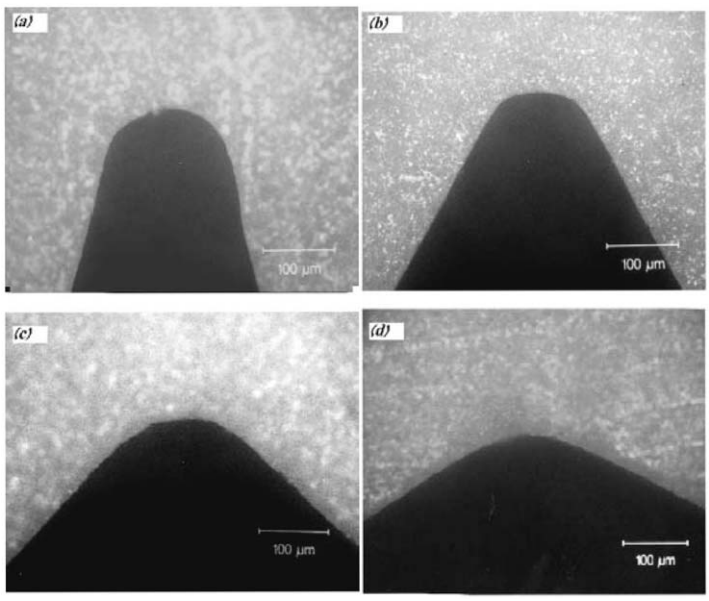

Figure 7. The 0.1 mm notch tip radius profile for different notch angles; (a) 30°, (b) 60°, (c) 90°, (d) 120°.

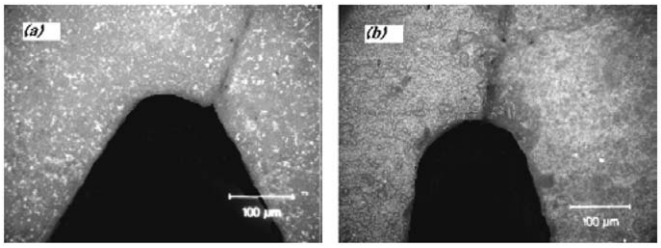

Figure 8. Crack initiation at the edge (a), or at the notch root (b).

Table 6. Summary of the experimental results for PMMA. All results except the two having $\omega = 45°$ are from Dunn et al. (1997b)

P	SED (0.0158 mm)	$A_1 s_{11}^{(1)}(90°)$ computed by (12)	$A_1 s_{11}^{(1)}(90°)$ computed by (9)	$(A_1)_{cr} s_{11}^{(1)}(90°)$ experiments
N	$\frac{\text{N}}{\text{m}^2}$		MPa $\times$ m$^{1-\alpha_1}$	
$\omega = 45°, \alpha_1 = 0.5050$				
376	5286756	0.427	0.432	0.586
379	5382800	0.427	0.432	0.591
$\omega = 60°, \alpha_1 = 0.5122$				
597	5390215	0.469	0.471	0.563
613	5683008	0.469	0.471	0.578
613	5683008	0.469	0.471	0.578
611	5645982	0.469	0.471	0.576
457	6164536	0.469	0.471	0.600
475	6659708	0.469	0.471	0.624
450	5977146	0.469	0.471	0.591
441	5740440	0.469	0.471	0.579
296	4311136	0.469	0.471	0.502
316	4913610	0.469	0.471	0.534
316	4913610	0.469	0.471	0.534
308	4667772	0.469	0.471	0.521
268	5919545	0.469	0.471	0.586
256	5401490	0.469	0.471	0.560
250	5151263	0.469	0.471	0.547
261	5614547	0.469	0.471	0.571

with the notch tip (see details by Yosibash and Szabó, 1995) and the generalized stress intensity factors A_ℓ's (see Szabó and Yosibash, 1996). In all cases the convergence of the solution in energy norm as well as the convergence in the GSIF was monitored and guaranteed to be within 2% relative error.

Table 7. Summary of the experimental results for PMMA from Dunn et al. (1997b)

P	SED (0.0158 mm)	$A_1 s_{11}^{(1)}(90°)$ computed by (12)	$A_1 s_{11}^{(1)}(90°)$ computed by (9)	$(A_1)_{cr} s_{11}^{(1)}(90°)$ experiments
N	$\frac{\text{N}}{\text{m}^2}$		MPa $\times$ m$^{1-\alpha_1}$	
$\omega = 90°, \alpha_1 = 0.5445$				
691	6369229	0.713	0.693	0.877
691	6369229	0.713	0.693	0.877
680	6168060	0.713	0.693	0.863
495	6072337	0.713	0.693	0.853
490	5950282	0.713	0.693	0.845
488	5901807	0.713	0.693	0.841
397	6355569	0.713	0.693	0.873
406	6646931	0.713	0.693	0.893
410	6778549	0.713	0.693	0.901
310	6431300	0.713	0.693	0.878
319	6810633	0.713	0.693	0.904
319	6810633	0.713	0.693	0.904
$\omega = 120°, \alpha_1 = 0.6157$				
875	6326762	1.717	1.604	2.011
886	6486834	1.717	1.604	2.036
886	6486834	1.717	1.604	2.036
880	6400874	1.717	1.604	2.022
652	5971698	1.717	1.604	1.951
660	6119142	1.717	1.604	1.975
646	5862296	1.717	1.604	1.933
671	6324814	1.717	1.604	2.008
468	4881352	1.717	1.604	1.764
521	6049561	1.717	1.604	1.964
521	6049561	1.717	1.604	1.964
519	6003203	1.717	1.604	1.956
321	3830550	1.717	1.604	1.564
340	4297431	1.717	1.604	1.656
339	4272189	1.717	1.604	1.651
345	4424756	1.717	1.604	1.681

4.1. Analysis of the Alumina-7%Zirconia test results

To check the validity of Novoshilov–Seweryn and Leguillon's criteria the GSIF has been computed at the failure point using K_{Ic} and σ_c, by Equations (9) and (12), respectively, and the predicted results were compared to the GSIF at failure. The values for $K(\omega)$ used in Leguillon's law is taken from Table 3. For the Alumina-7% Zirconia, $K_{I_c} = 4.1$ MPa$\sqrt{\text{m}}$ (see

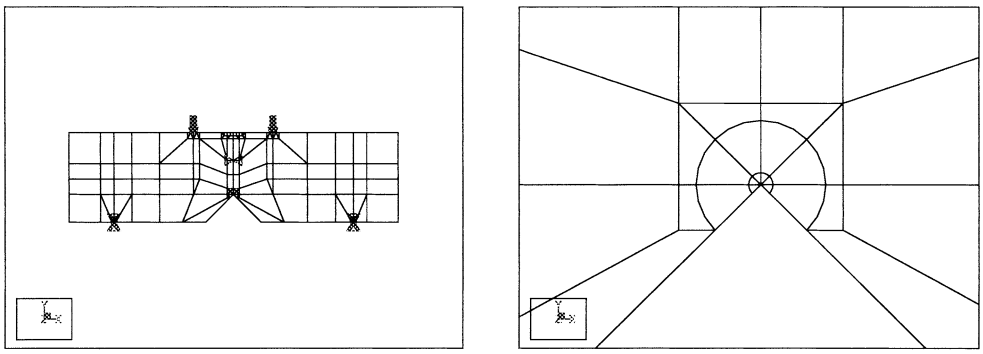

Figure 9. FE mesh for a $\omega = 90^\circ$ specimen. On the left the whole model, on the right the zoomed region around the singular point.

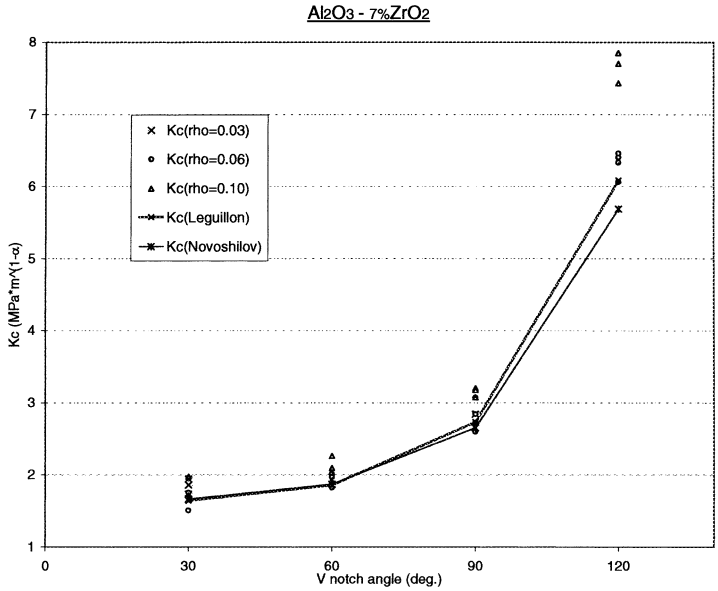

Figure 10. Predicted GSIFs (k_c) at failure by using Novoshilov and Leguillon's criteria, and GSIFs in tested Alumina-7%Zirconia specimens.

also Rosa et al., 1998) and $\sigma_c = 290$ MPa. The predicted values (independent of the V-notch radius) and the GSIF at failure (computed as $k_c = A_1 \times s_{11}^{(1)}(\theta = 90^\circ)$) are summarized in the last three columns of Table 5. These results are also plotted in Figure 10, and show a good correlation between the predicted values (by Leguillon and Novoshilov–Seweryn failure laws) and experimental observations.

As noticed, the validity of both tested criteria is very good at small opening angles, and deteriorates as the opening angle increases. Also both criteria assume a sharp V-notch tip therefore as the V-notch radius ρ increases the prediction is less accurate. This trend is best illustrated in Figure 11 where the GSIF at failure for the specimens having $\omega = 90^\circ$ are plotted as a function of ρ.

Using the eigen-pairs, the A_1 and the integration radius computed by (21) $R_{\text{mat}} = 0.062$ mm, we computed the SED at the instance of failure (denoted by $\text{SED}_{cr}[0.062\text{ mm}]$) and it is summarized in the fourth column of Table 5. The chosen R_{mat} is four times larger com-

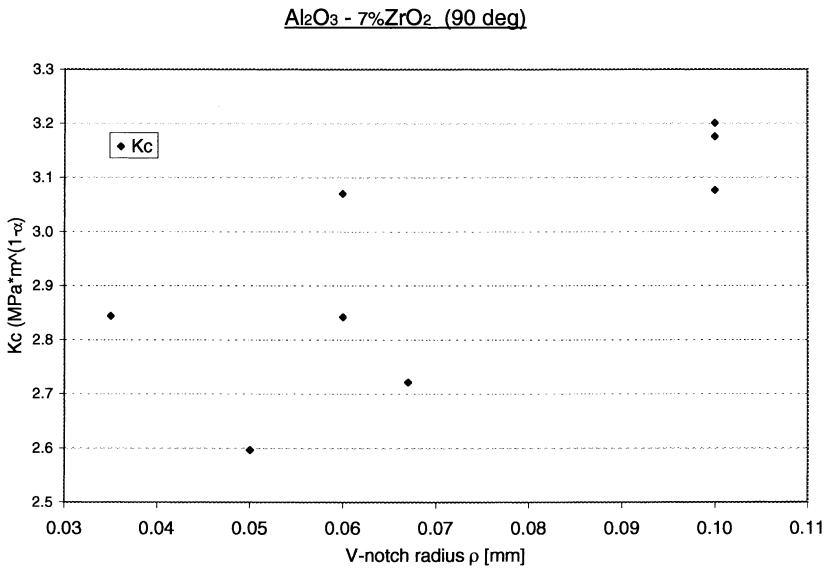

Figure 11. GSIFs as a function of ρ for the $\omega = 90°$ at failure for Alumina-7%Zirconia.

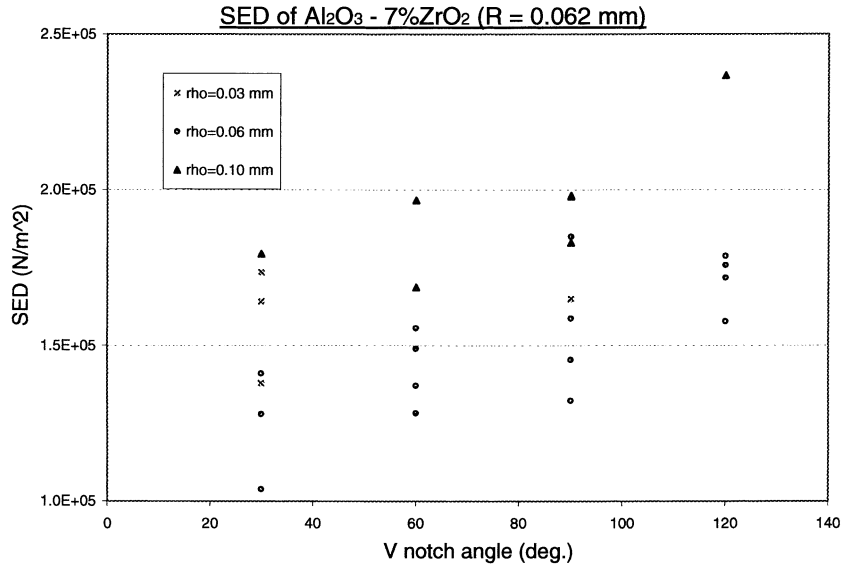

Figure 12. SED_{cr}[0.062 mm] in tested Alumina-7%Zirconia specimens.

pared to the approximated plastic radius, which is $r_p = 1/\pi\,(K_{Ic}/\sigma_c)^2 = 0.0155$ mm. SED_{cr}[0.062 mm] has been computed by using A_1 and the first eigen-pair, and once again by using the stress and strain tensors in the circular region surrounding the V-notch tip. The differences in the two results have been less than 3% in all cases, thus ensuring that the first term in the asymptotic expansion suffices to describe the quantity of interest with good accuracy. The SED_{cr}[0.062 mm] as a function of the V-notch opening angle ω is shown in Figure 12.

Because the SED is proportional to the square of A_1, the sensitivity of the results to changes in this parameter is more pronounced. Computing $\text{SED}[0.062\,\text{mm}]_{\text{crack}} = \text{SED}[0.062\,\text{mm}]_{\text{straight}}$

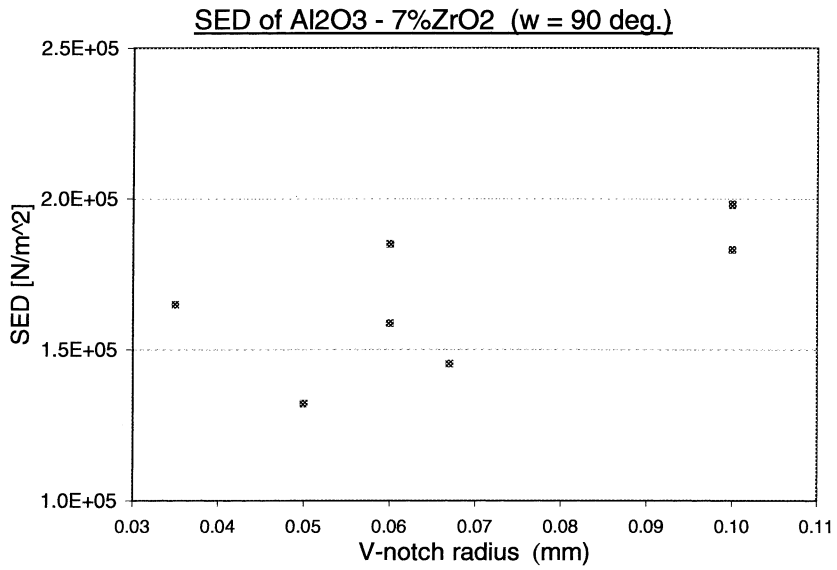

Figure 13. $\mathrm{SED_{cr}}[0.062\ \mathrm{mm}]$ for the $\omega = 90°$ Alumina-7%Zirconia specimens as a function of ρ.

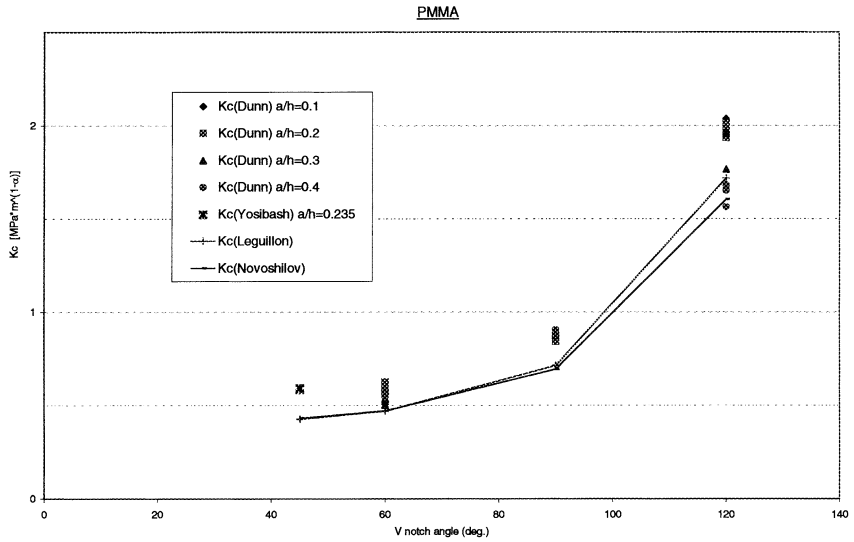

Figure 14. Predicted GSIFs at failure by using Novoshilov and Leguillon's criteria, and GSIFs in PMMA specimens.

$\approx 120,100\ \mathrm{N\ m^{-2}}$], it is clear that values of obtained $\mathrm{SED}[0.062\ \mathrm{mm}]_{cr}$ for all angles are within the anticipated range. Of course that the V-notch radius causes a higher SED_{cr} as the calculated SED (assuming $\rho = 0$). The $\mathrm{SED}[R]_{cr}$ at any R can be easily computed from the data presented herein by:

$$\mathrm{SED}[R]_{cr} = \left(\frac{R}{0.062\ \mathrm{mm}}\right)^{2\alpha_1 - 2} \mathrm{SED}[0.062\ \mathrm{mm}]_{cr}.$$

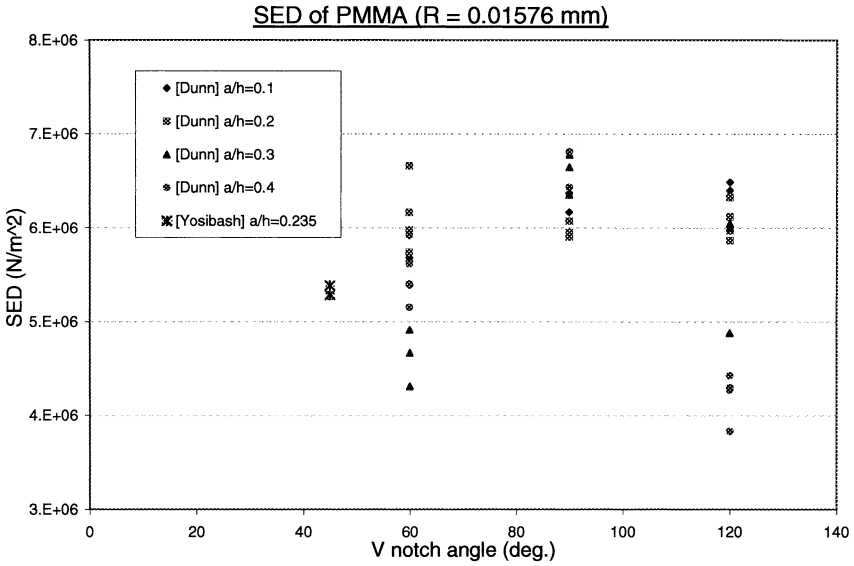

Figure 15. SED_{cr}[0.0158 mm] in PMMA specimens.

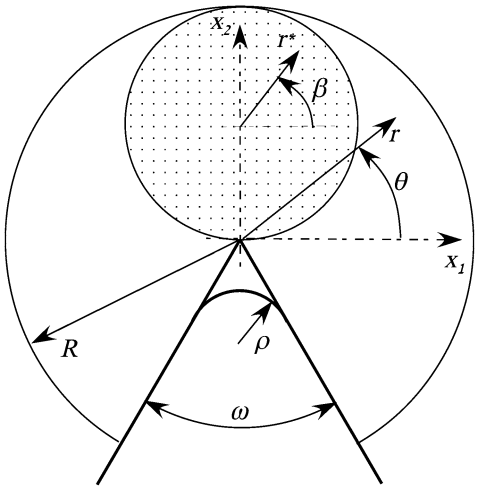

Figure 16. The new integration domain for computing SED.

The influence of ρ on the critical SED was also examined and depicted for the case of $\omega = 90^\circ$ in Figure 13. Because the values of ρ are close to these of R_{mat}, its influence is pronounced.

4.2. Analysis of the PMMA tests

Similarly to the analysis described in previous subsection, the validity of Novoshilov–Seweryn and Leguillon's criteria was also evaluated for the PMMA specimens. The values for $K(\omega)$ used in Leguillon's law is taken from II. For the PMMA material, $K_{I_c} = 1.028$ MPa$\sqrt{\mathrm{m}}$, $\sigma_c = 124$ MPa, $E = 2.3$ GPa, and $\nu = 0.36$ (see Dunn et al., 1997b). The predicted values and the GSIF at failure are summarized in the last three columns of Tables 6 and 7. These results are also plotted in Figure 14, and also show a good correlation of the predicted values

Table 8. Values of ℓ_0, d_0 and R_{mat} for PMMA and $Al_2O_3 - 7\%ZrO_2$ (and Duraluminum)

ω	ℓ_0 from (11) [mm]		d_0 from (8) [mm]			R_{mat} from (21) [mm]	
	PMMA	Al_2O_3-7%ZrO_2	PMMA	Al_2O_3-7%ZrO_2	Duraluminum[a]	PMMA	Al_2O_3-7%ZrO_2
30°	0.0105	0.031	0.0431	0.127	3.89	0.0158	0.062
45°	0.0106	0.031	0.0431	0.127	3.89	0.0158	0.062
60°	0.0108	0.032	0.0431	0.127	3.89	0.0158	0.062
90°	0.121	0.036	0.0431	0.127	3.89	0.0158	0.062
120°	0.146	0.043	0.0431	0.127	3.89	0.0158	0.062

[a]The value of $\sigma_c = 705$ MPa and $K_{Ic} = 55.14$ MPA$\sqrt{\text{m}}$ were used for evaluation of d_0, reported by Seweryn (1994).

and experimental observations. Because several specimens with notch depth to hight ratio a/h have been used by Dunn et al. (1997b), we list them all in Figures 14 and 15.

Again, the validity of both criteria tested is good at small opening angles, and deteriorates as the opening angle increases.

SED in the vicinity of the singular points has been also computed, and summarized in the second column of Tables 6 and 7. For the PMMA, the integration radius computed by (21) and used in our computations is $R_{\text{mat}} = 0.0158$ mm. The plastic radius for the PMMA is approximately $r_p = 0.0215$ mm which is the same order of magnitude as $R_{\text{mat}} = 0.0158$ mm. The SED_{cr}[0.0158 mm] as a function of the V-notch opening angle ω is shown in Figure 15. The values of $\text{SED}[0.0158\text{ mm}]_{\text{crack}} = \text{SED}[0.0158\text{ mm}]_{\text{straight}} \approx 3,340,000$ [N m^{-2}], which is a lower bound to the SED obtained in the experiments (again probably due to the V-Notch radius).

5. Conclusions

The validity of three failure criteria proposed in the last decade for predicting failure initiation at V-notch sharp tips has been examined and compared with experimental observations. The experiments include; loading of specimens made of two kinds of elastic materials (PMMA – a polymer, and Al_2O_3-7%ZrO_2, a composite ceramic) in three and four-points, so to produce mode I stress field in the vicinity of the notch tip. To quantify the influence of ρ on the failure initiation, specimens having different tip radii have been selected. All failure criteria assume a mathematical sharp tip, namely a small blunt tip (with a tip radius denoted by ρ) showing a higher generalized stress intensity factor as compared to the predicted values. Nevertheless, both the Novoshilov-Seweryn and Leguillon criteria seem to predict well the observed failures, however, as the opening angle increases, their validity deteriorates. This may be attributed to the non-exact measurement of σ_c, and the blunt tip radius. Leguillon criterion outperforms the Novoshilov–Seweryn criterion, and it has been refined to include ρ dependency so to match better the experimental observations - see Leguillon and Yosibash (2003). The Novoshilov-Seweryn criterion has been also considered for hyperbolic and elliptic notches with intrinsic blunted tips by Seweryn and Mróz (1995), but had not been compared to experimental observations.

Table 8 summarizes the assumed crack length increment ℓ_0 of Leguillon criterion, the path over which the stress is averaged d_0 in case of the Novoshilov–Seweryn criterion for the two elastic brittle materials considered, and R_{mat} used in our computations. The values show that

indeed ℓ_0, d_0 and R_{mat} are small and of comparative order of magnitude. Computing d_0 for Duraluminum (last column in Table 8), a material used in one of the experiments documented by Seweryn (1994), shows that it is of a larger magnitude compared to PMMA and Al_2O_3-7%ZrO_2. This value may be at the limit of the assumption of small d_0 thus for Duraluminum the predictions using either one of the above criteria may be slightly off.

The proposed SED criterion is more similar to the Dunn criteria in terms of the needed values of the critical SED for a large range of ω's. However, it is not unit dependent, and does not require the knowledge of K_{Ic} or σ_c for the material of interest. A practical application of the SED criterion, for predicting failure initiation in electronic devices under thermo-elastic loading is provided by Yosibash et al. (2003).

If chosen to be used, one can compute R_{mat} and obtain a SED which is independent of the re-entrant opening angle. We have seen that the predicted SED_{cr} is a lower estimate of the experimental observations, and the scattering in SED_{cr} is wide. These two effects can be reduced by using the square root of the SED as the failure criterion, and taking into account the V-notch radius tip ρ. The SED failure criterion may be improved by choosing a seemingly better integration domain to be the shaded circle shown in Figure 16, having a radius of $R/2$, and centered at $R/2$ away from the V-notch tip. Future investigations will assess the benefits of integrating the strain energy in this domain, in respect with obtaining a smaller scatter and a smaller variation in SED independent of the V-notch opening angle. Having the eigen-pairs and GSIFs in terms of r, θ, all which is needed is to express these in terms of r^*, β by:

$$r = \sqrt{2r^*(1 + \sin\,\beta)}, \quad \theta = \arctan\left(\frac{1 + \sin\,\beta}{\cos\,\beta}\right),$$

and perform an integration over $R/2 \geq r^* \geq 0$ and $2\pi \geq \beta \geq 0$. The applicability of the SED criterion to cases of mixed mode loading is under investigation, and its validity (assessed by experimental observations) will be documented in the future. Also, the explicit dependency of the the V-notch tip radius ρ on the SED is a subject of further investigation.

Acknowledgements

The authors would like to thank Mr Gal Amar for his help with FE analyses and Mr Moshe Kupiec for his help in performing the experiments. This research has been performed under VATAT-VEE grant number 84154201-86/02.

References

Amar, G. and Yosibash, Z. (2000). p-FEM for formulating an elastic criterion for predicting mechanical failures at 2-D singular points. In: *p-FEM2000, May 31-June 2: Summaries of Papers.* St. Louis, MO, USA, p. 15.

Dempsey, J.P. (1995). Power-logarithmic stress singularities at bi-material corners and interface cracks. *Journal Adhesion Sci. Technol.* **9**(2), 253–265.

Dunn, M.L., Suwito, W. and Cunningham, S. (1997a). Fracture initiation at sharp notches: Correlation using critical stress intensities. *International Journal Solids and Structures* **34**(29), 3873–3883.

Dunn, M.L., Suwito, W., Cunningham, S. and May, C.W. (1997b). Fracture initiation at sharp notches under mode I, mode II, and mild mixed mode loading. *International Journal of Fracture* **84**, 367–381.

Griffith, A.A. (1921). The phenomena of rupture and flow in solids. *Philosophical Tran. Roy. Soc. London, Ser A* **221**, 163–198.

Hattori, T. (1991). A stress singularity parameter approach for evaluating the adhesive strength of single-lap joints. *International Journal of Japanese Soc. Mech. Eng., Ser. I* **34**(3), 326–331.

Hattori, T., Sakata, S. and Murakami, G. (1989). A stress singularity parameter approach for evaluating the interfacial reliability of plastic encapsulated LSI Devices. *Journal of Electronic Packaging* **111**, 243–248.

Irwin, G.R. (1957). Analysis of stresses and strains near the end of a crack transversing a plate. *Trans. ASME, Jour. Appl. Mech.* **24**, 361–364.

Lazzarin, P. and Zmabardi, R. (2001). A finite-volume-energy based approach to predict the static and fatigue behavior of components with sharp V-shaped notches. *International Journal of Fracture* **112**, 275–298.

Leguillon, D. (2001). A critetion for crack nucleation at a notch in homogeneous materials. *C.R. Acad. Sci. Paris, Ser IIb* **329**, 97–102.

Leguillon, D. (2002). Strength or toughness? A criterion for crack onset at a notch. *Eur. J. of Mechanics A/Solids* **21**, 61–72.

Leguillon, D. and Yosibash, Z. (2003). Crack onset at a V-Notch. Influence of the notch tip radius. *International Journal of Fracture*, **122**, 1–21.

Novozhilov, V. (1969). On a necessary and sufficient criterion for brittle strength. *Jour. Appl. Math. Mech. (Translation of PMM)* **33**(2), 212–222.

Reedy, J.E.D. and Guess, T.R. (1995). Butt tensile joint strength: interface corner stress i intensity factor prediction. *Jour. Adhesion Science Technology* **9**, 237–251.

Rice, J.R. (1988). Elastic fracture mechanics concepts for interfacial cracks. *Trans. ASME, Jour. Appl. Mech.* **55**, 98–103.

Rosa, L., Fernandes, J. and Duarte, I. (1998). Subcritical crack growth in three engineering ceramics under biaxial conditions. In: *ECF12 – Fracture from Defects* (Edited by M. Brown, E. de los Rios, and K. Miller), Volume I EMAS Publishing, pp. 509–514.

Seweryn, A. (1994). Brittle fracture criterion for structures with sharp notches. *Eng. Frac. Mech.* **47**(5), 673–681.

Seweryn, A. and Lukaszewicz, A. (2002). Verification of brittle fracture criteria for elements with V-shaped notches. *Eng. Frac. Mech.* **69**, 1487–1510.

Seweryn, A. and Mróz, Z. (1995). A non-local stress failure condition for structural elements under multiaxial loading. *Eng. Frac. Mech.* **51**, 955–973.

Sih, G. and Macdonald, B. (1974). Fracture mechanics applied to engineering problems – strain energy density fracture criterion. *Eng. Fracture Mechanics* **6**, 361–386.

Suo, Z. (1989). Mechanics of interface fracture. Ph.D. thesis, Harvard University, Cambridge, Massachusetts, USA.

Suwito, W. and Dunn, M.L. (1998). Fracture initiation at sharp notches in single crystal silicon. *Jour. Appl. Physics* **83**, 3574–3582.

Szabó, B.A. and Babuška, I. (1991). *Finite Element Analysis*. John Wiley & Sons, New York.

Szabó, B.A. and Yosibash, Z. (1996). Numerical analysis of singularities in two-dimensions. Part 2: Computation of the generalized flux/stress intensity factors. *Int. Jour. Numer. Meth. Engrg.* **39**(3), 409–434.

Williams, M.L. (1952). Stress singularities resulting from various boundary conditions in angular corners of plates in extension. *Trans. ASME, Jour. Appl. Mech.* **19**, 526–528.

Yosibash, Z. (1994). Numerical analysis of singularities and first derivatives for elliptic boundary value problems in two-dimensions. Ph.D. thesis, Sever Institute of Technology, Washington University, St. Louis, Missouri, USA.

Yosibash, Z., Adan, O., Shneck, R. and Atlas, H. (2003). Thermo-mechanical failure criterion at the micron scale in electronic devices. *Int. Jour. Fracture*. **122**, 47–64.

Yosibash, Z. and Szabó, B.A. (1995). Numerical analysis of singularities in two-dimensions. Part 1: Computation of eigenpairs. *Int. Jour. Numer. Meth. Engrg.* **38**(12), 2055–2082.

Appendix A. Computation of the critical SED$[\mathbf{R}]_{\mathbf{crack}}$ for a crack and SED$[\mathbf{R}]_{\mathbf{straight}}$ for a straight edge, and a material characteristic integration radius $\mathbf{R_{mat}}$

The two extreme values of the critical SED$[R]$ are obtained for the case of a crack ($\omega = 0°$) and a straight edge ($\omega = 180°$). We first derive these values for an isotropic material, under mode I loading, and then use these equations to determine a material characteristic integration radius denoted by R_{mat}.

COMPUTATION OF THE CRITICAL $\mathrm{SED}[R]_{\mathrm{straight}}$

For a specimen with a straight edge, failure occurs at the instance when the remote uniaxial stress is equal to σ_c. In this case the state of stresses at any point will be $\sigma_{11} = \sigma_c$ and other stress components are zero. The strain energy can be expressed as:

$$\mathcal{U}(\mathbf{u})[R] = \tfrac{1}{2}b\int_0^{\pi}\int_0^{R}\sigma_{jk}\varepsilon_{jk}r\,\mathrm{d}\theta\,\mathrm{d}r = \tfrac{1}{2}b\int_0^{\pi}\int_0^{R}\sigma_c\frac{\sigma_c}{E}r\,\mathrm{d}\theta\,\mathrm{d}r = \frac{b}{4E}\pi R^2\sigma_c^2, \tag{23}$$

so that we finally obtain the upper limit to the SED:

$$\mathrm{SED}[R]_{\mathrm{straight}} = \frac{\sigma_c^2}{2E}. \tag{24}$$

COMPUTATION OF THE CRITICAL $\mathrm{SED}[R]_{\mathrm{crack}}$

Under mode I loading, for a specimen containing a crack, the stress tensor at the instance of fracture in the vicinity of a crack tip is given by:

$$\begin{aligned}
\sigma_{11} &= \frac{K_{Ic}}{\sqrt{2\pi r}}\cos\frac{\theta^*}{2}\left[1-\sin\frac{\theta^*}{2}\sin\frac{3\theta^*}{2}\right],\\
\sigma_{22} &= \frac{K_{Ic}}{\sqrt{2\pi r}}\cos\frac{\theta^*}{2}\left[1+\sin\frac{\theta^*}{2}\sin\frac{3\theta^*}{2}\right],\\
\sigma_{12} &= \frac{K_{Ic}}{\sqrt{2\pi r}}\sin\frac{\theta^*}{2}\cos\frac{\theta^*}{2}\cos\frac{3\theta^*}{2},
\end{aligned} \tag{25}$$

where the coordinate system r, θ^* is located so that $\theta* = 0$ is along the x_2 axis. Expressing the strains in terms of stresses using the plane-strain constitutive law, (26) becomes:

$$\mathcal{U}(\mathbf{u})[R] = \tfrac{1}{2}\frac{(1+\nu)b}{E}\int_{-\pi}^{\pi}\int_0^{R}\left\{(1+\nu)\left[\sigma_{11}^2+\sigma_{22}^2\right]-2\nu\sigma_{11}\sigma_{22}+2\sigma_{12}\right\}r\,\mathrm{d}r\,\mathrm{d}\theta^*. \tag{26}$$

Substitute (25) in the expression of the strain energy (26):

$$\mathcal{U}(\mathbf{u})[R] = \frac{b(1+\nu)(5-8\nu)}{8E}K_{Ic}^2R, \tag{27}$$

one finally obtains the lower limit to the SED:

$$\mathrm{SED}[R]_{\mathrm{crack}} = \frac{(1+\nu)(5-8\nu)}{8\pi RE}K_{Ic}^2. \tag{28}$$

DETERMINATION OF THE MATERIAL CHARACTERISTIC INTEGRATION RADIUS R_{mat}

Following Lazzarin and Zambardi (2001), and requiring that the SED is independent of the opening angle ω, then for $\omega = 0$ and for $\omega = \pi$ one should obtain the same SED. Thus, by equating (24) with (28), one obtains:

$$\frac{\sigma_c^2}{2E} = \frac{(1+\nu)(5-8\nu)}{8\pi RE}K_{Ic}^2. \tag{29}$$

Equation (29) holds for a specific integration radius R_{mat}, which is given after trivial algebraic manipulation:

$$R_{\mathrm{mat}} = \frac{(1+\nu)(5-8\nu)}{4\pi}\left(\frac{K_{Ic}}{\sigma_c}\right)^2. \tag{30}$$

Appendix B. Summary of all tested Alumina-7% Zirconia specimens

In the Tables 9 and 10 we summarize all our experimental results for the Al_2O_3 - 7%ZrO_2 specimens.

Table 9. Summary of the experiments for all tested Alumina-7%Zirconia specimens, and GSIFs (k_c)

Specimen	ρ mm	P N	E GPa	SED [0.062 mm] $\frac{\text{N}}{\text{m}^2}$	$A_1 s_{11}^{(1)}$ ($\theta = 90°$) computed by (12)	$A_1 s_{11}^{(1)}$ ($\theta = 90°$) computed by (9) MPa $\times$ $\text{m}^{1-\alpha_1}$	$(A_1)_{cr} s_{11}^{(1)}$ ($\theta = 90°$) experiments
$\omega = 30°, \alpha_1 = 0.501453$							
AO30003-16	0.031	1815	350	173547	1.643	1.662	1.942
AO30003-15	0.034	1933	350	193343	1.643	1.662	2.050
30-FPB-0.03-6	0.040	1799	356.7	155653	1.627	1.662	1.858
30-TPB-0.03-1	0.040	1594	350	206743	1.643	1.662	2.126
30-TPB-0.03-3	0.040	1436	350	164253	1.643	1.662	1.863
AO30003-11	0.041	1628	350	137811	1.643	1.662	1.732
AO30003-12	0.041	1942	350	195107	1.643	1.662	2.059
AO30003-13	0.041	2060	350	219061	1.643	1.662	2.182
AO30003-14	0.041	1942	350	196070	1.643	1.662	2.064
30-FPB-0.03-5	0.043	1662	356.7	124459	1.627	1.662	1.661
AO30006-12	0.060	1628	350	144150	1.643	1.662	1.771
AO30006-13	0.060	1628	350	140944	1.643	1.662	1.751
AO30006-14	0.060	1560	350	129963	1.643	1.662	1.682
30-FPB-0.1-1	0.060	1717	356.7	111336	1.627	1.662	1.573
30-TPB-0.1-4	0.060	1439	356.7	127912	1.627	1.662	1.690
30-TPB-0.1-5	0.060	1413	350	103800	1.643	1.662	1.509
AO3001-12	0.100	1844	350	179506	1.643	1.662	1.976
AO3001-13	0.100	1805	350	162298	1.643	1.662	1.879
AO3001-14	0.100	1991	350	216510	1.643	1.662	2.170
AO3001-15	0.100	1962	350	208776	1.643	1.662	2.131
$\omega = 60°, \alpha_1 = 0.512221$							
60-FPB-0.03-3	0.055	1874	356.7	160487	1.842	1.870	2.062
60-TPB-0.03-4	0.055	1736	350	230972	1.859	1.870	2.457
60-FPB-0.1-2	0.055	1962	356.7	164484	1.842	1.870	2.119
60-FPB-0.1-4	0.055	1953	356.7	167227	1.842	1.870	2.106
60-FPB-0.1-1	0.060	1972	356.7	175081	1.842	1.870	2.153
15.4.02 - 11	0.060	1753	350	155625	1.859	1.870	2.010
15.4.02 - 12	0.060	1701	350	148996	1.859	1.870	1.967
15.4.02 - 13	0.060	1721	350	150637	1.859	1.870	1.979
15.4.02 - 14	0.060	1658	350	140199	1.859	1.870	1.909
15.4.02 - 15	0.060	1603	350	128253	1.859	1.870	1.826
15.4.02 - 16	0.060	1526	350	120240	1.859	1.870	1.768
15.4.02 - 18	0.060	1680	350	137102	1.859	1.870	1.888
60-FPB-0.1-5	0.070	1895	350	161609	1.859	1.870	2.052
A06001-12	0.100	1785	350	168763	1.859	1.870	2.095
A06001-13	0.100	1903	350	196644	1.859	1.870	2.262
A06001-14	0.100	1913	350	199512	1.859	1.870	2.280

Table 10. (Continued) Summary of the experiments for all tested Alumina-7%Zirconia specimens, and GSIFs (k_c)

Specimen	ρ mm	P N	E GPa	SED[0.062 mm] $\frac{\text{N}}{\text{m}^2}$	$A_1 s_{11}^{(1)}$ ($\theta = 90°$) (12)	$A_1 s_{11}^{(1)}$ ($\theta = 90°$) (9) MPa $\times$ m$^{1-\alpha_1}$	$(A_1)_{cr} s_{11}^{(1)}$ ($\theta = 90°$)
$\omega = 90°, \alpha_1 = 0.5444837$							
AO90003-12	0.028	2080	350	178957	2.732	2.655	2.984
90-FPB-0.03-1	0.033	1810	350	148275	2.732	2.655	2.744
AO90003-13	0.034	1884	350	172346	2.732	2.655	2.955
AO90003-14	0.034	1785	350	154451	2.732	2.655	2.799
90-FPB-0.03-5	0.035	1853	338.5	164962	2.774	2.655	2.844
90-FPB-0.03-2	0.037	1821	350	148427	2.732	2.655	2.746
AO90003-11	0.041	1805	350	158736	2.732	2.655	2.837
90-FPB-0.03-3	0.042	1847	356.7	153300	2.708	2.655	2.815
90-FPB-0.03-4	0.042	1838	356.7	152188	2.708	2.655	2.804
90-TPB-0.03-7	0.050	1292	350	132235	2.732	2.655	2.596
90-FPB-0.03-6	0.060	1878	350	161330	2.732	2.655	2.862
90-FPB-0.06-4	0.060	1974	350	150037	2.732	2.655	2.761
90-FPB-0.06-5	0.060	2144	350	181154	2.732	2.655	3.033
90-TPB-0.06-1	0.060	1523	350	158707	2.732	2.655	2.842
90-TPB-0.06-2	0.060	1642	350	184986	2.732	2.655	3.071
90-TPB-0.06-3	0.067	1461	350	145375	2.732	2.655	2.722
90-FPB-0.1-5	0.100	2167	356.7	183066	2.708	2.655	3.077
90-FPB-0.1-6	0.100	2244	356.7	198267	2.708	2.655	3.201
90-FPB-0.1-7	0.100	2478	356.7	242519	2.708	2.655	3.540
90-TPB-0.1-3	0.100	1724	350	197814	2.732	2.655	3.176
$\omega = 120°, \alpha_1 = 0.6157311$							
120-FPB-0.03-6	0.060	2551	350	219358	6.087	5.688	7.143
120-TPB-0.03-5	0.062	1962	350	171724	6.087	5.688	6.329
120-FPB-0.03-4	0.068	2580	350	191434	6.087	5.688	6.672
120-FPB-0.06-4	0.080	2442	350	162729	6.087	5.688	6.152
120-TPB-0.06-1	0.080	1927	350	175779	6.087	5.688	6.403
120-TPB-0.06-2	0.080	1805	350	157698	6.087	5.688	6.065
120-TPB-0.06-3	0.080	1958	350	178687	6.087	5.688	6.456
AO12006-12	0.083	2659	350	205967	6.087	5.688	6.923
AO12006-11	0.096	2266	350	154212	6.087	5.688	5.988
120-TPB-0.03-1	0.100	1893	350	177860	6.087	5.688	6.441
120-FPB-0.1-1	0.100	2931	350	270141	6.087	5.688	7.926
120-FPB-0.1-4	0.100	2655	350	222233	6.087	5.688	7.190
120-FPB-0.1-3	0.100	2928	350	255128	6.087	5.688	7.705
120-FPB-0.1-5	0.100	2892	350	265188	6.087	5.688	7.853
120-TPB-0.1-6	0.100	2053	350	236806	6.087	5.688	7.435